Am J Nucl Med Mol Imaging 2024;14(2):122-133
www.ajnmmi.us /ISSN:2160-8407/ajnmmi0154931

Original Article

[^{99m}Tc]Tc-labeled cyc-DX600-HYNIC as a SPECT probe for ACE2-specific pancreatic cancer imaging

Pan Zhou[1,2*], Zheng Li[2*], Danni Li[3], Shuai Xue[1,2], Rou Li[3], Lan Zhang[2], Qingyun Bai[1], Xiao Li[2,3,4]

[1]School of Chemistry and Bioengineering, Yichun University, Yichun 336000, Jiangxi, China; [2]Shanghai Institute of Applied Physics, Chinese Academy of Sciences, Shanghai 201800, China; [3]Department of Nuclear Medicine, Shanghai Changhai Hospital, Shanghai 200433, China; [4]Department of Nuclear Medicine, Pudong Hospital, Fudan University, Shanghai 201399, China. [*]Equal contributors.

Received December 13, 2023; Accepted April 2, 2024; Epub April 25, 2024; Published April 30, 2024

Abstract: As a regulator in renin-angiotensin-aldosterone system, angiotensin-converting enzyme 2 (ACE2) closely correlated with tumor progression of pancreatic cancer, meantime, was easily affected by a variety of factors. [^{99m}Tc]Tc-cyc-DX600 SPECT was established as an ACE2-specific imaging protocol to figure out the ACE2 status in pancreatic tumor. BALB/C-NU mice were used to prepare the subcutaneous cell derived xenograft (CDX) models with HEK-293T or HEK-293T/hACE2 cells to validate ACE2 specificity of [^{99m}Tc]Tc-cyc-DX600 SPECT and establish SPECT imaging protocol. On the basis of [^{99m}Tc]Tc-cyc-DX600 SPECT and [^{18}F]F-FDG PET/CT, ACE2-dependence on tumor size and tumor metabolism were further verified on orthotopic pancreatic cancer model with KPC cells. Immunohistochemical analysis was used to demonstrate the findings on ACE2 SPECT. [^{99m}Tc]Tc-cyc-DX600 was of superior tumor uptake in HEK-293T/hACE2 CDX than wild type (6.74 ± 0.31 %ID/mL vs 1.83 ± 0.26 %ID/mL at 1.5 h post injection (p.i.); 3.14 ± 0.31 %ID/mL vs 1.16 ± 0.15 %ID/mL at 4.5 h p.i.). For the CDX models with PANC-1 cells, a significant negative correlation between the slope of tumor volume and tumor uptake was observed (r = -0.382 for the 1-4th day; r = -0.146 for the 1-5th day; r = -0.114 for the 1-6th day; r = -0.152 for the 1-7th day; but $P > 0.05$ for all). For orthotopic pancreatic cancer model, the linear correlation between FDG PET and ACE2 SPECT of the pancreatic lesions was negative (r = -0.878), the quantitative values of ACE2 SPCET was positively correlated with the volume of primary lesions (r = 0.752) and also positively correlated with the quantitative values of ACE2 immunohistochemical analysis (r = 0.991). Conclusively, [^{99m}Tc]Tc-cyc-DX600 SPECT is an ACE2-specific imaging protocol with clinical translational potential, adding multidimensional information on the disease progression of pancreatic cancer.

Keywords: ACE2, pancreatic cancer, [^{99m}Tc]Tc-cyc-DX600, functional imaging, single photon emission computed tomography, renin-angiotensin-aldosterone system

Introduction

Due to the complex anatomical location of the pancreas, the lack of obvious early symptoms and the high invasiveness, pancreatic cancer is difficult to detect and make a definite diagnosis at an early stage, and the diagnosis made in a late stage is also often not all-inclusive [1, 2], leading to a poor prognosis and a low survival rate [3, 4]. The appropriate diagnosis is crucial for the treatment of pancreatic cancer patients, but the non-invasive or non-specific means are of few information on molecular levels [5-7]. For example, the widely used [^{18}F]F-FDG PET/CT, although used in visualizing tumor tissues, inflammatory lesions and benign tumors, the metabolic characteristics are often indistinguishable in clinical diagnosis of pancreatic cancer [8]. Herein, the establishment of a molecular imaging method is warranted to improve the current diagnosis efficiency on pancreatic cancer.

The local expression of regulatory components of renin-angiotensin-aldosterone system (RAAS) has been demonstrated in a variety of cancer cells and tissues, including pancreatic, lung, breast, prostate and cervical cancer [9, 10]. The pancreas is an important component of the RAAS, and ACE2 disorders directly associate with pathological changes, which usually constitute a causal relationship [11, 12]. Accompanying by abnormal DNA methylation, ACE2 expression is significantly up-regulated not only in the pancreatic cancer, but also in other malignant tumors such as colon adenocarcinoma, papillary cell carcinoma of the kidney, rectal adenocarcinoma, gastric adenocarcinoma and lung adenocarcinoma [13]. In consideration of the interaction with treatment, ACE2 also served as an indicator in tumor invasiveness, tumorigenesis and progression [14-17]. Taking non-small cell lung cancer as an example, it has been demonstrated that ACE2 overexpression may potentially suppress invasion and angiogenesis in non-small cell lung cancer after the development of acquired platinum resistance [18]. Furthermore, it has been reported that reduction of ACE2 expression by RNA interference promotes the proliferation of cultured pancreatic cancer cells, suggesting that ACE2 inhibition may have clinical potential as a novel molecular target for the treatment of pancreatic ductal adenocarcinoma and reduction of cell proliferation [19]. In addition, there is evidence that ACE2 is a prognostic biomarker for gallbladder cancer [14]. These studies suggest that measuring ACE2 activity may be a helpful tool to indicate the diagnosis and prognosis of cancer patients.

https://doi.org/10.62347/VFHT4078

Recently, the COVID-19 pandemic has brought renewed attention to the important role of ACE2 in the progression of various diseases, which included the long-COVID, cardivascular diseases and cancers [20, 21]. Aiming to figuring out the diseased pathology and facilitating diagnosis, our research group and some researchers have used ACE2-targeted molecular imaging as a diagnostic mode for ACE2-related diseases [22-24]. The known ACE2-specific inhibitors, DX600 and MLN-4760, as well as some bioactive protein, such as spike protein of virus, were developed as an ACE2-tracer of molecular imaging protocols, but still of space for improvements on translational medicine [15, 24-28]. DX600 is a peptidic inhibitor that selectively binds to ACE2, demonstrating a strong affinity in the nanomolar range, while exhibiting a unique inhibition mechanism involving both competitive and non-competitive modes. Unlike common linear polymers, cyclic peptide polymers with cyclic structures show higher stability, which can be attributed to their ring topology and their lack of chain ends. In this study, the molecular probe constructed demonstrated a cyclic structure (cyc-DX600) through precursor design, the sulfhydryl group of the DX600 cysteine condensed into the cyclic structure, with the formation of a disulfide bond enhancing the structural stability of the precursor for the corresponding cyc-DX600 system. Radionuclides with a longer diagnostic window or reduced plasma ACE2 uptake show clinical translational potential in enhancing the quality of ACE2-targeted molecular imaging [29]. Therefore, This study synthesized [^{99m}Tc]Tc-cyc-DX600 as an ACE2-specific SPECT imaging tracer. The feasibility of [^{99m}Tc]Tc-cyc-DX600 to assess ACE2 expression in tumors.

Materials and methods

Synthesis and characterization of [^{99m}Tc]Tc-cyc-DX600

cyc-DX600-HYNIC was custom-synthesized as the labeling precursor by QYAOBIO with chemical purity of *ca.* 90%. For the synthesis of [^{99m}Tc]Tc-cyc-DX600, 20 μg cyc-DX600-HYNIC, 1 mg Tricine and 0.5 mg ethylenediamine-N,N'-diacetic acid (EDDA) were dissolved in 1 mL 0.01 M PBS. Immediately after that, around 1 mL newly-eluted sodium pertechnetate [Na^{99m}TcO$_4$] injection and 100 μg $SnCl_2{\cdot}2H_2O$ in diluted HCl were added in the solution, and then oscillated at 100°C for 10 min.

For characterization of chemical purity and radiochemical purity (RCP) of [^{99m}Tc]Tc-cyc-DX600, HPLC analysis was performed on an Agilent 1100 system equipped with a variable-wavelength UV detector and radio-detector connected in series. An analysis column (Wondasil C18 Superb 5 μm, 4.6 × 250 mm) was used with a flow rate of 1 mL/min, and parameters were set as solvent A: water with 0.1% TFA, solvent B: 100% acetonitrile, gradient details: 0-13 min, 33%-67% B, UV at 220 nm.

Cells culture

HEK-293T cells, HEK-293T cells with high expression of humanized ACE2 (hACE2) protein (HEK-293T/hACE2 cells) (OBiO Technology Ltd., Shanghai, China), PANC-1 cells and KPC cells were incubated in DMEM with 10% FBS. 100 μg/mL streptomycin and 100 U/mL penicillin were supplemented in the cluture medium, and cells were incubated with 5% CO_2 at 37°C.

Establishment and treatment of CDX models

All animal experiments were in accordance with the guidelines approved by the Ethics Committee of Pudong Hospital of Fudan University (Approval No.: 2023-MS-DS-08). BALB/C-NU mice (6 weeks old, male) and BALB/C mice (6 weeks old, male, only for KPC models) used in the study were purchased from SiPeiFuMice (Suzhou) Biotechnology Co., LTD., and then housed under appropriate environmental conditions (50% humidity, 22°C, lights on from 6:00 to 18:00) with free access to water and feed.

To establish the subcutaneous CDX models, HEK-293T cells, HEK-293T/hACE2 cells and PANC-1 cells, logarithmic growth phase were selected, digested and resuspended in 0.01 M PBS, respectively, then mixed with Matrigel (1:1 ratio) and stored temporarily at 4°C. 100 μL mixture (1×10^7 cells) were injected subcutaneously into the right sub-axilla of each mouse. Tumor volume was measured everyday, and imaging or treatment was performed when tumor size reached 300 μL.

Tumor growth curve analysis

For the CDX models with PANC-1 cells, tumor size and body weight of each mouse were measured and recorded every day. Volume was calculated by the following formula: tumor volume = length × width^2 × 0.5. A tumor growth curve was plotted as tumor volume versus time. To evaluate tumor growth over time, tumor volume slope in the tumor growth curve was calculated. The index of tumor progression was defined as the slope of linear regression between time length and tumor volume in a definite period.

Establishment of orthotopic pancreatic cancer model

For the establishment of orthotopic pancreatic cancer model, KPC cells derived from genetically engineered KPC-mice with spontaneous pancreatic ductal adenocarcinoma in mice was selected. Cells were digested and resuspended in 0.01 M PBS, and then mixed with Matrigel (1:1 ratio) and stored temporarily at 4°C. KPC cells were prepared at a density of 5×10^7/mL. Mice were anesthetized by inhalation with 2% isoflurane, and then the spleen and pancreas tail were exposed through an incision about 1 cm beside the left superior abdominis rectus muscle. 20 μL mixture was slowly injected into the tail of the pancreas. The microsyringe was removed, and the incision was closed with a 4-0 surgical line. After the mice were fully resuscitated, the mice were randomly grouped and fed in appropriate environmental conditions (50% humidity, 22°C, lights on from 6:00 to 18:00) with free

diet. About 6 weeks later, the tumor could grow to about 200 μL with potential multiple metastatic lesions.

[^{99m}Tc]Tc-cyc-DX600 SPECT of model mice

Mice were anesthetized by inhalation with 1.5-2% isoflurane, 15 MBq [^{99m}Tc]Tc-cyc-DX600 was injected into each HEK-293T and HEK-293T/hACE2 CDX mouse model via the tail vein. Mice were placed in the SPECT scanner (γ-CUBE, Molecubes, Belgium) for scanning at 1.5 h and 4.5 h after injection, separately. The SPECT images (algorithm, Maximum Likelihood Expectation Maximization; peak, 140 keV; isometric voxel size, 500 μm) were acquired for 28 min, and CT (X-CUBE, Molecubes, Belgium) images were subsequently acquired (algorithm, iterative; tube voltage: 50 kVp; tube current: 0.15 mA; isometric voxel size, 200 μm; exposure time, 300 ms). Accounting for image quality and time efficiency, 1.5 h was selected for the following scans of pancreatic cancer models.

Blocking experiments were conducted to investigate the receptor specificity of [^{99m}Tc]Tc-cyc-DX600. The blocking group was pre-injected with 50-fold molar excess of non-radiolabeled precursor one hour in advance. Imaging experiments were performed at 1.5 h after injection, with the same procedure as above.

To further study the effects of [^{99m}Tc]Tc-cyc-DX600 evaluated ACE2 expression with pancreatic cancer tumor aggressiveness and growth. The CDX models with PANC-1 cells were injected intravenously with 15 MBq [^{99m}Tc]Tc-cyc-DX600 per mouse, and the SPECT scanning were performed with the same procedures as above.

Image reconstruction was performed in VivoQuant software (Invicro) to form hybrid SPECT images in transverse, coronal and sagittal planes. Regions of interest (ROI) were drawn on the tumors, and the pancreatic tumor size were measured in the orthotopic pancreatic cancer model via draming volume of interest manually (VOI). The tumor-to-muscle ratio (T/M) was calculated by dividing the tumor uptake (%ID/mL) of the tumor by that of the background (muscle). The tumor (pancreas)-to-heart ratio (T/H) was calculated by dividing the tumor uptake (%ID/mL) of the tumor (pancreas) by that for heart.

[^{18}F]F-FDG PET/CT of orthotopic pancreatic cancer model

[^{18}F]F-FDG PET/CT images were scanned and collected by FDG PET/CT scanner (Inveon, Siemens). After inhalation of isoflurane anesthetic, 120 μCi [^{18}F]F-FDG was injected intravenously to each mouse that were then placed in the prone position in the central area of FDG PET/CT device and then scanned at 45 min after injection. FDG PET/CT images were acquired for 15 min (Energy windows: 350-650 kev; Time windows: 3.432 nsec), and CT images were acquired for one minute (tube voltage: 80 kVp; tube current: 0.5 mA; average frame: 1.0; fliter thickness: 1 mm). Reconstruction of statically acquired data in the 3D-OSEM MAP system to obtain clear images. FDG PET/CT workstation provided a quantification value of [^{18}F]F-FDG uptake as maximum standardized uptake value (SUV_{max}). The uptake was quantified by drawing ROIs, including pancreas tumor and major metastatic lesions.

After the imaging examination, the orthotopic pancreatic cancer model were euthanized, and the pancreas and major metastatic lesions were collected. The expression of ACE2 in pancreatic tumor and metastatic lesions was detected by immunohistochemistry staining.

Immunohistochemistry

Tumor tissue and major metastatic organs were analyzed by immunohistochemistry using anti-ACE2 antibodies following a standard protocol after SPECT imaging was completed. Tumor tissue and major metastatic organs were fixed in 4% paraformaldehyde, paraffin-embedded tissues were sectioned (4 μm) and deparaffinized. Tissue sections were dewaxed and hydrated, and the sections were injected into antigen repair solution (0.01 mM sodium citrate buffer) at 60°C overnight. The blocking solution was discarded, and anti-ACE2 antibody diluted in the appropriate proportion was added onto the sections overnight at 4°C. The configured secondary antibody was dropped onto the tissue sections, incubated at room temperature for 1 h. The reaction was carried out with DAB as a chromogen. Then the sections were counterstained with hematoxylin. The immunohistochemical images were observed by inverted fluorescence microscope (Olympus BX43, Olympus Corporation, Japan), and the data were processed by Image-Pro Plus software (Version 6.0.0.260, Media Cybernetics Corporation, USA).

Statistical analysis

[^{99m}Tc]Tc-cyc-DX600 uptakes were quantified as %ID/mL or SUV_{max}, and [^{18}F]F-FDG uptakes were quantified as SUV_{max}. Values were shown as mean ± SD. A 2-tailed t-test was used for comparisons between the two groups. For the CDX model with PANC-1 cells, linear regression was performed between the index of tumor progression and tumor uptake of [^{99m}Tc]Tc-cyc-DX600. For the orthotopic pancreatic cancer model, linear regression was performed between SUV_{max} of FDG PET/CT images and SUV_{max} of [^{99m}Tc]Tc-cyc-DX600 in the pancreatic lesions; linear regression was performed between the tumor uptake of [^{99m}Tc]Tc-cyc-DX600 and the lesional volume of pancreas; linear regressions were performed between average optical density (AOD, AOD = IOD/Area) and tumor uptake of [^{99m}Tc]Tc-cyc-DX600 in the primary lesions and main metastases. The data were analyzed by SPSS 26.0 statistical software, and *P*-values of less than 0.05 were defined as statistically significant. OriginPro 2019b software was used to plot graphs.

A

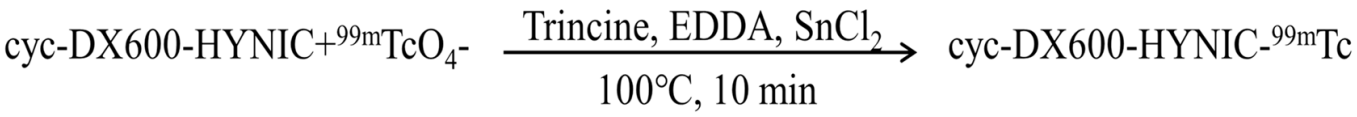

B

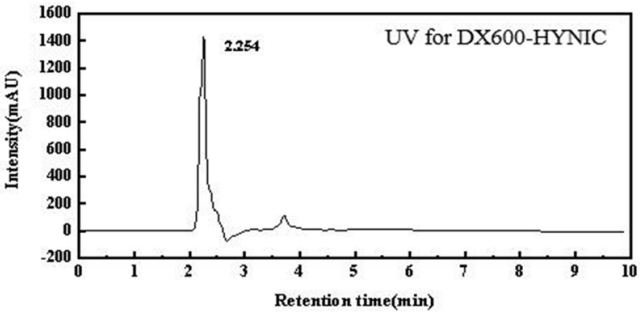

C

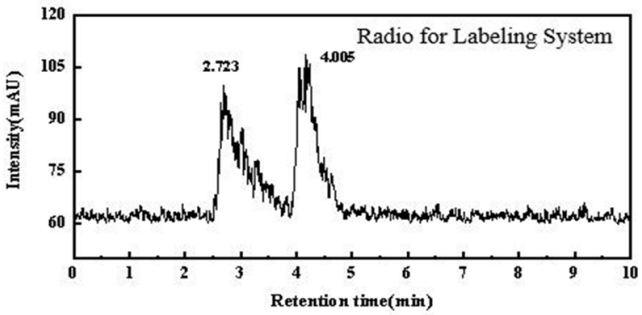

Figure 1. (A) The schematic procedure of [^{99m}Tc]Tc-cyc-DX600; HPLC chromatograms of cyc-DX600-HYNIC (UV-trace, 220 nm, B and γ-trace, C).

Results

Characterization of [^{99m}Tc]Tc-cyc-DX600

Figure 1A provided the schematic synthesis of [^{99m}Tc]Tc-cyc-DX600. The whole procedure, including synthesis, purification and quality control, can be completed in less than 25 min. In **Figure 1B**, HPLC spectrum of precursor cyc-DX600-HYNIC showed a purity of 93.0 ± 0.5% and a retention time of 2.254 min.

The precursor can be labeled by ^{99m}Tc with the coactive ligands Tricine and EDDA to obtain the labeled molecule [^{99m}Tc]Tc-cyc-DX600 with a labeling rate of 57.2 ± 1.5%, serving as the targeted tracer of ACE2. **Figure 1C** was the radioactivity detection of the labeling reaction solution with the retention time of the labeled molecule at 2.723 min, and the peak at 4.005 min was the radioactive signal of free ^{99m}Tc.

A step of purification with C18-based extraction was needed before use, so as to acquire the product with a radiochemical purity of higher than 95%.

ACE2-spcificity of [^{99m}Tc]Tc-cyc-DX600

The tumor uptake of [^{99m}Tc]Tc-cyc-DX600 at two studied time points (1.5 h, 4.5 h) were shown in **Figure 2**. Tumor uptake of [^{99m}Tc]Tc-cyc-DX600 was significantly higher in ACE2-positive HEK-293T/hACE2 CDX (6.74 ± 0.31 %ID/mL at 1.5 h p.i.) than in ACE2-negative HEK-293T CDX (1.83 ± 0.26 %ID/mL at 1.5 h p.i.). Tumor uptake of [^{99m}Tc]Tc-cyc-DX600 was still higher in ACE2-positive HEK-293T/hACE2 CDX (3.14 ± 0.31 %ID/mL at 4.5 h p.i.) than in ACE2-negative HEK-293T CDX (1.16 ± 0.15 %ID/mL at 4.5 h p.i.) (**Figure 2A**). The results demonstrated the specific localization of the probe to ACE2-positive tissues. For the images acquired at 1.5 h p.i., there was a significant difference on the ratio of T/M (15.72 ± 0.72 for HEK-293T/hACE2 CDX, and 4.27 ± 0.60 for HEK-293T CDX, $P < 0.001$). Furthermore, the ratio of T/M of HEK-293T/hACE2 CDX (5.85 ± 1.07) were significantly higher than those of HEK-293T CDX (1.64 ± 0.22, $P < 0.001$) at 4.5 h p.i. Thereafter, 1.5 h post injection was used as the scan point for ACE2-related imaging of tumor models, even though 4.5 hours post injection still could be a valid time for differential diagnosis of ACE2.

In blocking experiments, it was noted that at 1.5 h after injection, the radioactivity concentration in the tumor of blocked mice was significantly reduced to 5.15 ± 0.06 %ID/mL, but still a higher uptake than the one of ACE2-negative xenografts (**Figure 2B**).

Although the morphology of the cells and intercellular matrix were essentially the same as proved by hematoxylin and eosin (H&E) staining, the positive ACE2 expression (AOD: 0.34 ± 0.09) of HEK-293T/hACE2 CDX and the negative ACE2 expression (AOD: 0.19 ± 0.02) of HEK-293T CDX were clearly showed on IHC (**Figure 2C**, **2D**), which further confirmed the capacity of [^{99m}Tc]Tc-cyc-DX600 SPECT in evaluating tumor ACE2 condition. In short, these data indicated that [^{99m}Tc]Tc-cyc-DX600 can specifically target and bind to tissues with high ACE2 expression.

Image analysis of the CDX models with PANC-1 cells

Tumor growth curve graphs demonstrated a progressive increase in the tumor volume over time (**Figure 3A**). Importantly, analysis of the ACE2 SPECT imaging data from the CDX models with PANC-1 cells revealed a negative relationship between tumor uptake of ACE2 SPECT and index of tumor progression (r = -0.382 for the 1-4th day; r = -0.146 for the 1-5th day; r = -0.114 for the 1-6th day; r = -0.152 for the 1-7th day; $P > 0.05$ for all) (**Figure 3B**). From the results of the correlation analysis, ACE2 SPECT/CT was of a more predictive value in the early

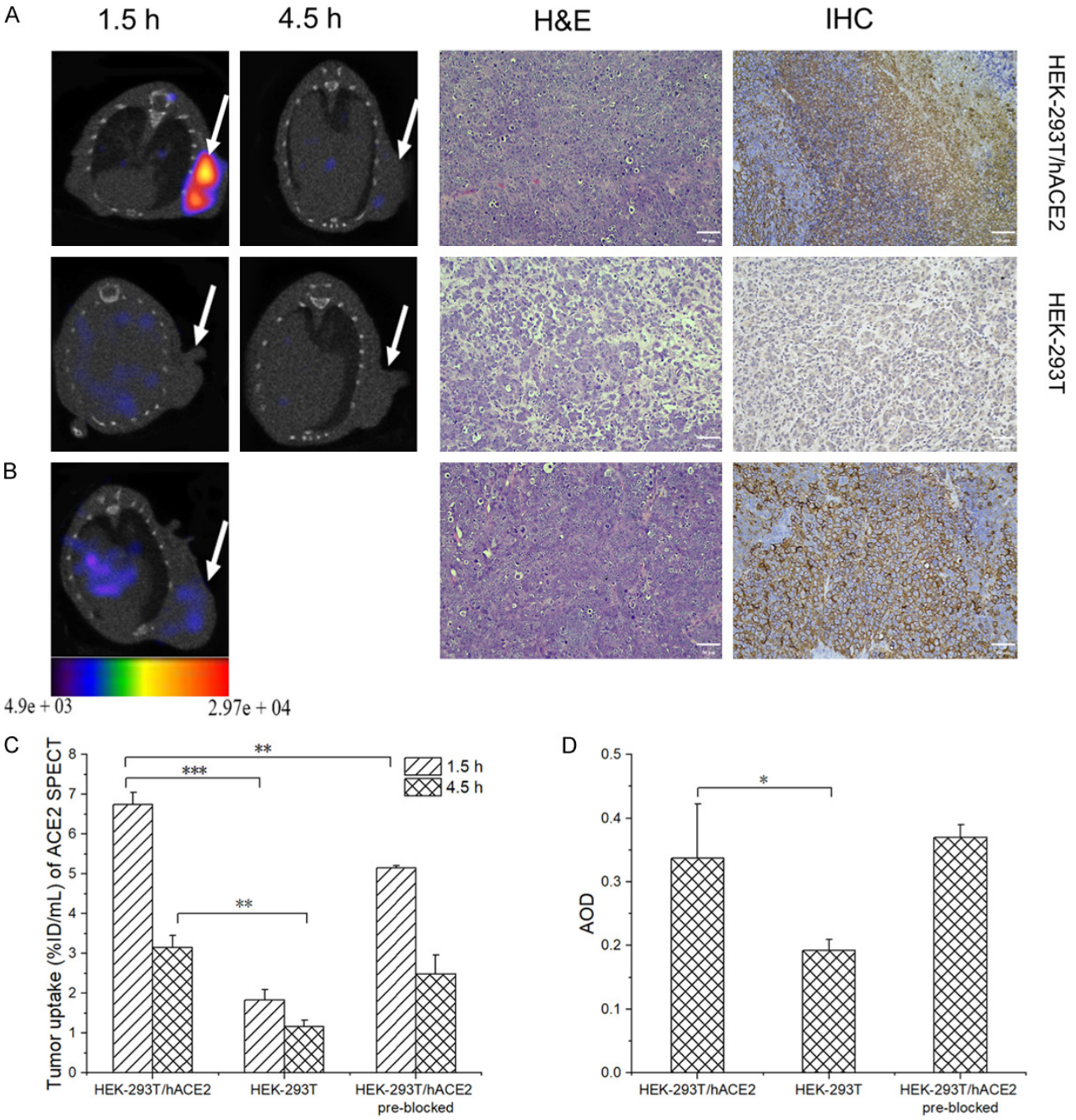

Figure 2. [^{99m}Tc]Tc-cyc-DX600 SPECT and verification of ACE2 targeting. A. The SPECT images of HEK-293T/hACE2 and HEK-293T CDX, the corrvesponding H&E and IHC staining of HEK-293T/hACE2 and HEK-293T CDX; B. The SPECT images of [^{99m}Tc]Tc-cyc-DX600 of HEK-293T/hACE2 CDX blocked with DX600; and the corresponding HE and IHC staining of HEK-293T/hACE2 CDX blocked with DX600 (magnification ×200, scale bar: 50 μm); C. The summary of tumor uptake (%ID/mL) of ACE2-positive, ACE2-negative and pre-blockage ACE2-positive xenografts; D. The summary of AOD of ACE2-positive, ACE2-negative and pre-blockage ACE2-positive xenografts (*$P < 0.05$, **$P < 0.01$, ***$P < 0.001$).

phase in monitoring tumor growth and aggressiveness. Therefore, as the tumor volume grows over time, tumors with low expression of ACE2 showed high aggressiveness, which further confirmed the sensitivity of [^{99m}Tc]Tc-cyc-DX600 as an ACE2-specific imaging agent in this CDX model.

Correlation between pancreatic uptake and tumor progression characteristics in orthotopic pancreatic cancer model

Both at the imaging level and the data analysis level, the high tumor uptake (0.05 ± 0.02, n = 4) was observed in

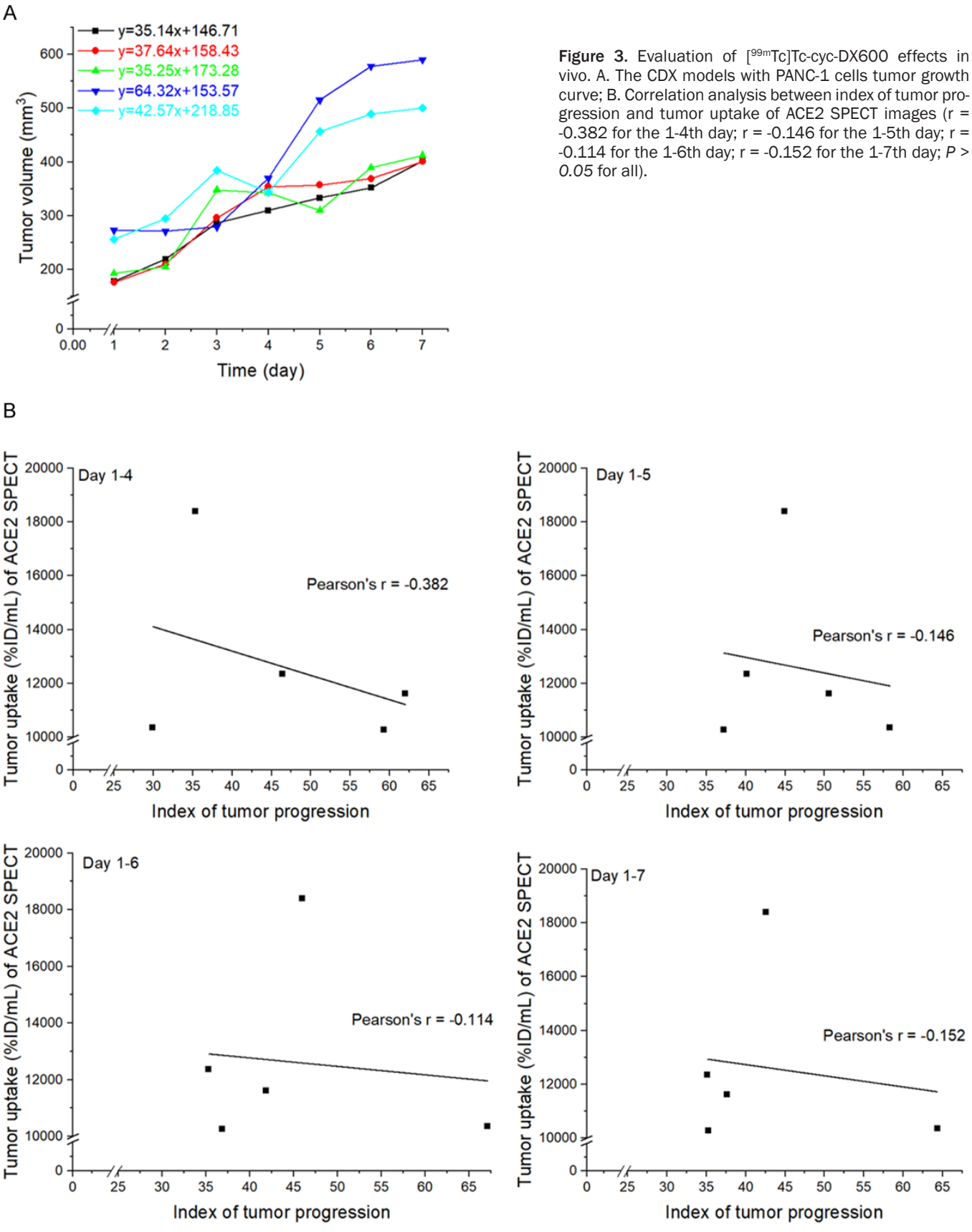

Figure 3. Evaluation of [^{99m}Tc]Tc-cyc-DX600 effects in vivo. A. The CDX models with PANC-1 cells tumor growth curve; B. Correlation analysis between index of tumor progression and tumor uptake of ACE2 SPECT images (r = -0.382 for the 1-4th day; r = -0.146 for the 1-5th day; r = -0.114 for the 1-6th day; r = -0.152 for the 1-7th day; $P > 0.05$ for all).

the pancreas of orthotopic pancreatic cancer model compared to the in vivo distribution of normal mice in the control group (**Figure 4A**). The linear correlation between SUV_{max} of FDG PET/CT images and SUV_{max} of ACE2 SPECT images of the pancreas was negative (r = -0.878, $P > 0.05$) (**Figure 4B**). In contrast, as a functional imaging that

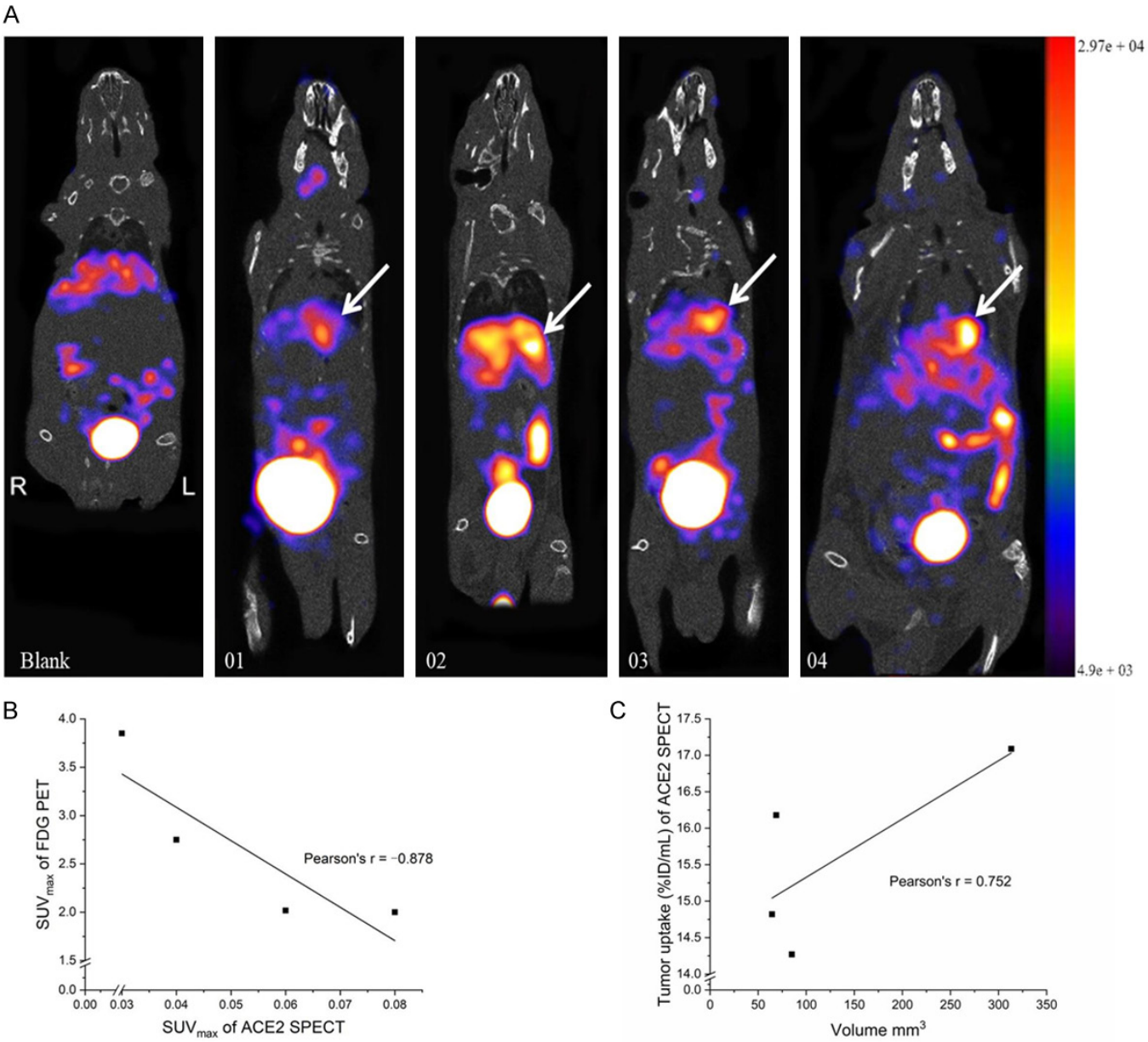

Figure 4. In vivo [^{99m}Tc]Tc-cyc-DX600 of orthotopic pancreatic cancer model. A. [^{99m}Tc]Tc-cyc-DX600 images of mice were obtained in coronal (The numbers "01", "02", "03", "04" represent different mice of the same group, respectively), the arrow indicated the location of the tumor; B. Correlation analysis between SUV$_{max}$ of FDG PET/CT images and tumor uptake of ACE2 SPECT images of the pancreas (r = -0.878, *P* > *0.05*); C. Correlation analysis between %ID/mL and volume of the pancreatic lesion (r = 0.752, *P* > *0.05*).

can reflect ACE2 expression, the linear correlation between SUV$_{max}$ of ACE2 SPECT and volume defined as voxels with high tracer uptake of the pancreas was positive (r = 0.752, *P* > *0.05*) (**Figure 4C**). The linear correlation between SUV$_{max}$ of FDG PET/CT images and tracer uptake of ACE2 SPECT images demonstrated the accuracy of ACE2 SPECT imaging, which further demonstrated the usability of ACE2 SPECT in dynamic monitoring of ACE2 expression in pancreatic cancer.

ACE2 SPECT imaging of tumors and immunohistochemistry assays in an orthotopic pancreatic cancer model

To evaluate the feasibility of [^{99m}Tc]Tc-cyc-DX600 as a probe for tumor detection *in vivo*, SPECT imaging was conducted in an orthotopic pancreatic cancer model. **Figure 5** manifested the monitoring images of [^{99m}Tc]Tc-cyc-DX600 SPECT and [^{18}F]F-FDG PET/CT for ACE2-expression, respectively. SPECT images showed high uptake of [^{99m}Tc]Tc-cyc-DX600 in the stomach (4.00 %ID/mL), pancreas (4.86 %ID/mL), the FDG PET/CT images displayed more intense uptake of [^{18}F]F-FDG in the stomach (SUV$_{max}$: 1.80), pancreas (SUV$_{max}$: 14.40). SPECT images showed significant accumulation in the pancreatic lesion (T/H = 2.30, **Figure 5A**), while PET/CT images showed moderate uptake in the primary lesion (T/H = 0.90, **Figure 5B**). The same ACE2 expression of the primary lesions and major metastatic lesions in orthotopic pancreatic cancer model were confirmed by IHC on ACE2 (**Figure 5C**, **5D**). Here, a positive correlation between the quantitative values of

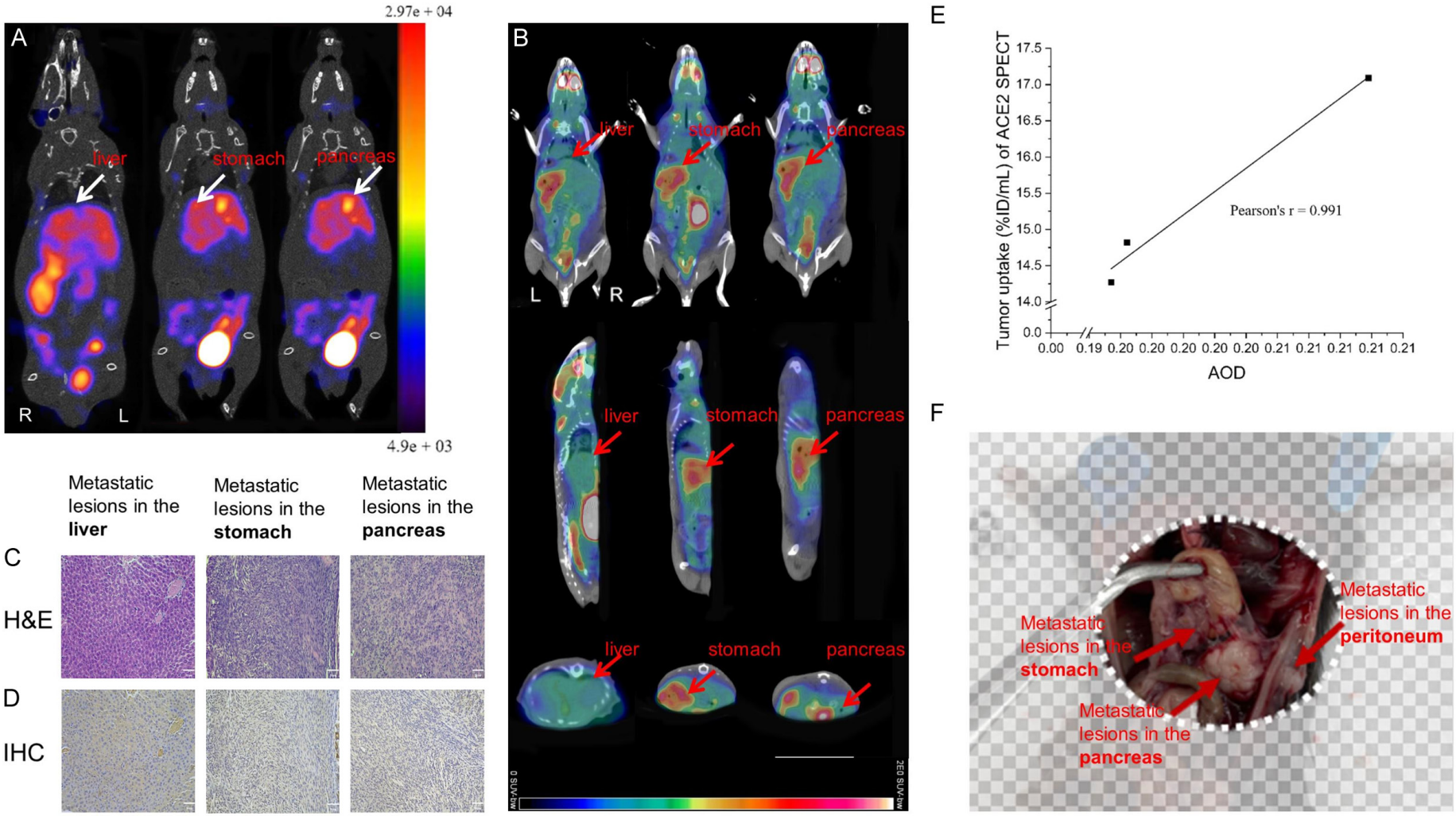

Figure 5. Comparison of SPECT imaging and FDG PET/CT imaging, H&E and immunohistochemical staining of sections from orthotopic tumor of pancreatic cancer. (A) [^{99m}Tc]Tc-cyc-DX600 SPECT images (Coronal section); (B) [^{18}F]F-FDG PET/CT images (Coronal section, Sagittal section, Transverse section); H&E and immunohistochemical staining of pancreas and major metastatic organs sections were analyzed (HE, C; IHC, D, magnification ×200, scale bar: 50 μm); (E) Correlation between tumor uptake (%ID/mL) and ACE2 immunohistochemical expression in pancreas (r = 0.991, *P* > *0.05*); (F) Gross inspection of orthotopic pancreatic cancer model with primary lesion and main metastasis marked.

ACE2 SPCET and ACE2 immunohistochemical expression in pancreatic lesion (r = 0.991, *P* > *0.05*, **Figure 5E**). Primary pancreatic tumors, gastric metastases and peritoneal metastases were clearly visualized on the gross anatomical drawings of the mice (**Figure 5F**). This correlation further validated the specificity of [^{99m}Tc]Tc-cyc-DX600 for ACE2 expression in pancreatic cancer. Therefore, SPECT imaging was precise in the initial evaluation of ACE2 expression and thus indirectly assessed the severity of metastatic lesions.

Discussion

Currently, [^{18}F]F-FDG PET/CT has been used as an important complement to conventional imaging for the diagnosis of pancreatic cancer [30]. However, a retrospective analysis of 232 patients with suspected pancreatic ductal adenocarcinoma found that FDG PET detected only 50% of early pancreatic cancers [31]. The lack of early symptoms of pancreatic cancer has limited the practical use of FDG PET/CT in early diagnosis. In addition, [^{18}F]F-FDG PET/CT has limitations, including difficulty in differentiating tumor from mass pancreatitis and accurately assessing lymph node metastasis [32, 33]. We prepared Tc-99m-labeled cyc-DX600-HYNIC and evaluated [^{99m}Tc]Tc-cyc-DX600 as a pancreatic cancer imaging agent in experimental animals. [^{99m}Tc]Tc-cyc-DX600 SPECT was a potential clinical translation of ACE2-specific imaging protocol, which added multidimensional information about the disease progression of pancreatic cancer.

ACE2 is a member of RAAS family. Many components of RAAS are locally expressed in various cancer cells and tissues, including pancreatic cancer [34-38]. In addition to playing an important regulatory role in RAAS-related diseases, ACE2 is highly expressed in endothelial cells of the heart, kidneys, and testis and primarily degrades ANG II into angiotensin 1-7 (ANG 1-7), which is considered a vasodilator and involved in apoptosis and growth arrest, as opposed to ACE activity that produces ANG II and degrades ANG 1-9 [39-41]. ACE is an effective countermodulator against ACE2, which acts as a potential antitumor molecule in a variety of malignant diseases, including prostate cancer, HCC, and lung cancer [42-45]. Timely and accurate grasp of ACE2 expression is of great significance for understanding tumor progression.

Currently, most ACE2-targeted tracers are designed based on the DX600 that was modified and then labeled with ^{64}Cu, ^{68}Ga, ^{18}F [26, 46-50]. For the abundant radionuclides aggregated in the blood pool and kidneys, PET imaging agent based on ^{68}Ga is of a too short half-life, that goes against lowering the blood background [47, 48]. In this imaging protocol, with a half-life of 6.02 h, ^{99m}Tc is of a good prospect in the application of tumor imaging mainly through the advantages of urinary metabolism and corresponding high blood background clearance efficiency in the delayed phase of ACE2 SPECT. [^{99m}Tc]Tc-cyc-DX600 SPECT protocol was validated in the diagnosis of pancreatic tumor, and the applicable value and validity in several subtypes were manifested. When other confounding factors, such as the source of tumor and feeding conditions, were strictly confined, the size of tumor volume indicated the rate of growth. For individuals with a higher growth rate, local RAAS tended to exert an anticancer effect by upregulating ACE2 expression. Thus, as the disease progressed in mice, we observed a positive correlation between tumor uptake by ACE2 SPECT and the volume of primary pancreatic lesions in this study. Overall, RAAS is a complex system in regulating tumor growth, ACE2 PET provides a method to visualize the whole procedure. In a comprehensive view, the full map in the perspective of primary lesions, metastases, and adjacent normal tissues presented the diversity of tumor-associated ACE2 expression. In contrast, despite their recognized accuracy and status as the prevailing diagnostic method, molecular laboratory tests exhibit certain limitations in accurately identifying tumorous ACE2-related pathological alterations, particularly when undertaking a comprehensive evaluation of the entire organism. [^{99m}Tc]Tc-cyc-DX600 as an ACE2-specific imaging tracer could complement ^{18}F-FDG to provide a more comprehensive image. In this study, the functional imaging recorded the pancreatic cancer model at a molecular level, and the quantitative expression of ACE2 in most tumor has an important reference value for diagnosis [18, 19, 51-54]. ACE2 also served as a target of radionuclide drug conjugates, and cancer treatment was potentially benefited from the appropriate half-life and Auger electron energy suitable for target tumor radiotherapy [55, 56].

Although promising directions seem to put improvements in the diagnosis and treatment of pancreatic cancer within reach, further experimental studies, including more extensive animal models with patient-derived xenografts are needed to validate these improvements.

Conclusion

Tc-99m-labeled cyc-DX600-HYNIC was prepared and evaluated as a pancreatic cancer imaging agent in experimental animals. These data suggested that ACE2-specific molecular imaging can comprehensively evaluate the expression of ACE2 in pancreatic cancer, potential benefiting the appropriate diagnosis and optimal choice of treatment modality when compared to conventional imaging techniques.

Acknowledgements

This research was supported by the health technology project of Pudong New Area health committee (PW2023D-06) and the National Natural Science Foundation Youth Project (82202216) of China.

Disclosure of conflict of interest

None.

Address correspondence to: Qingyun Bai, School of Chemistry and Bioengineering, Yichun University, Yichun 336000, Jiangxi, China. E-mail: 110623@jxycu.edu.cn; Xiao Li, Shanghai Institute of Applied Physics, Chinese Academy of Sciences, Shanghai 201800, China. E-mail: lixiao@sinap.ac.cn

References

[1] Singh RR and O'Reilly EM. New treatment strategies for metastatic pancreatic ductal adenocarcinoma. Drugs 2020; 80: 647-669.

[2] Yang J, Xu R, Wang C, Qiu J, Ren B and You L. Early screening and diagnosis strategies of pancreatic cancer: a comprehensive review. Cancer Commun (Lond) 2021; 41: 1257-1274.

[3] Siegel RL, Miller KD, Wagle NS and Jemal A. Cancer statistics, 2023. CA Cancer J Clin 2023; 73: 17-48.

[4] Miller KD, Nogueira L, Devasia T, Mariotto AB, Yabroff KR, Jemal A, Kramer J and Siegel RL. Cancer treatment and survivorship statistics, 2022. CA Cancer J Clin 2022; 72: 409-436.

[5] Kanno A, Masamune A, Hanada K, Maguchi H, Shimizu Y, Ueki T, Hasebe O, Ohtsuka T, Nakamura M, Takenaka M, Kitano M, Kikuyama M, Gabata T, Yoshida K, Sasaki T, Serikawa M, Furukawa T, Yanagisawa A and Shimosegawa T; Japan Study Group on the Early Detection of Pancreatic Cancer (JEDPAC). Multicenter study of early pancreatic cancer in Japan. Pancreatology 2018; 18: 61-67.

[6] Luo B, Peng F, Hong M, Su S, Fang C, Yang X, Xia G and Li B. ERCP combined with tumor markers in differential diagnosis of pancreatic cancer and pseudotumor-like pancreatitis. J BUON 2019; 24: 1568-1573.

[7] Bunganič B, Laclav M, Dvořáková T, Bradáč O, Traboulsi E, Suchánek Š, Frič P and Zavoral M. Accuracy of EUS and CEH EUS for the diagnosis of pancreatic tumours. Scand J Gastroenterol 2018; 53: 1411-1417.

[8] Zhang Z, Jia G, Pan G, Cao K, Yang Q, Meng H, Yang J, Zhang L, Wang T, Cheng C and Zuo C. Comparison of the diagnostic efficacy of (68)Ga-FAPI-04 PET/MR and (18)F-FDG PET/CT in patients with pancreatic cancer. Eur J Nucl Med Mol Imaging 2022; 49: 2877-2888.

[9] Uemura H, Ishiguro H, Nakaigawa N, Nagashima Y, Miyoshi Y, Fujinami K, Sakaguchi A and Kubota Y. Angiotensin II receptor blocker shows antiproliferative activity in prostate cancer cells: a possibility of tyrosine kinase inhibitor of growth factor. Mol Cancer Ther 2003; 2: 1139-1147.

[10] Greco S, Muscella A, Elia MG, Salvatore P, Storelli C, Mazzotta A, Manca C and Marsigliante S. Angiotensin II activates extracellular signal regulated kinases via protein kinase C and epidermal growth factor receptor in breast cancer cells. J Cell Physiol 2003; 196: 370-377.

[11] Almutlaq M, Alamro AA, Alamri HS, Alghamdi AA and Barhoumi T. The effect of local renin angiotensin system in the common types of cancer. Front Endocrinol (Lausanne) 2021; 12: 736361.

[12] Deshayes F and Nahmias C. Angiotensin receptors: a new role in cancer? Trends Endocrinol Metab 2005; 16: 293-299.

[13] Chai P, Yu J, Ge S, Jia R and Fan X. Genetic alteration, RNA expression, and DNA methylation profiling of coronavirus disease 2019 (COVID-19) receptor ACE2 in malignancies: a pan-cancer analysis. J Hematol Oncol 2020; 13: 43.

[14] Xu J, Fan J, Wu F, Huang Q, Guo M, Lv Z, Han J, Duan L, Hu G, Chen L, Liao T, Ma W, Tao X and Jin Y. The ACE2/angiotensin-(1-7)/mas receptor axis: pleiotropic roles in cancer. Front Physiol 2017; 8: 276.

[15] Huang L, Sexton DJ, Skogerson K, Devlin M, Smith R, Sanyal I, Parry T, Kent R, Enright J, Wu QL, Conley G, DeOliveira D, Morganelli L, Ducar M, Wescott CR and Ladner RC. Novel peptide inhibitors of angiotensin-converting enzyme 2. J Biol Chem 2003; 278: 15532-15540.

[16] Meiners J, Jansen K, Gorbokon N, Büscheck F, Luebke AM, Kluth M, Hube-Magg C, Höflmayer D, Weidemann S, Fraune C, Möller K, Bernreuther C, Lebok P, Menz A, Jacobsen F, Clauditz T, Sauter G, Uhlig R, Wilczak W, Izbicki J, Perez D, Minner S, Burandt E, Krech T, Marx A, Simon R and Steurer S. Angiotensin-converting enzyme 2 protein is overexpressed in a wide range of human tumour types: a systematic tissue microarray study on >15,000 tumours. Biomedicines 2021; 9: 1831.

[17] Feng H, Wei X, Pang L, Wu Y, Hu B, Ruan Y, Liu Z, Liu J and Wang T. Prognostic and immunological value of angiotensin-converting enzyme 2 in pan-cancer. Front Mol Biosci 2020; 7: 189.

[18] Feng Y, Wan H, Liu J, Zhang R, Ma Q, Han B, Xiang Y, Che J, Cao H, Fei X and Qiu W. The angiotensin-converting enzyme 2 in tumor growth and tumor-associated angiogenesis in non-small cell lung cancer. Oncol Rep 2010; 23: 941-948.

[19] Feng Y, Ni L, Wan H, Fan L, Fei X, Ma Q, Gao B, Xiang Y, Che J and Li Q. Overexpression of ACE2 produces antitumor effects via inhibition of angiogenesis and tumor cell invasion in vivo and in vitro. Oncol Rep 2011; 26: 1157-1164.

[20] Li W, Moore MJ, Vasilieva N, Sui J, Wong SK, Berne MA, Somasundaran M, Sullivan JL, Luzuriaga K, Greenough TC, Choe H and Farzan M. Angiotensin-converting enzyme 2 is a functional receptor for the SARS coronavirus. Nature 2003; 426: 450-454.

[21] Yang Q, Hughes TA, Kelkar A, Yu X, Cheng K, Park S, Huang WC, Lovell JF and Neelamegham S. Inhibition of SARS-CoV-2 viral entry upon blocking N- and O-glycan elaboration. Elife 2020; 9: e61552.

[22] Ren F, Jiang H, Shi L, Zhang L, Li X, Lu Q and Li Q. (68)Ga-cyc-DX600 PET/CT in ACE2-targeted tumor imaging. Eur J Nucl Med Mol Imaging 2023; 50: 2056-2067.

[23] Wang Z, Liu Z, Yang L, Ding J, Wang F, Liu T, Yang Z, Wang C, Zhu H and Liu Y. Noninvasive mapping of angiotensin converting enzyme-2 in pigeons using micro positron emission tomography. Life (Basel) 2022; 12: 793.

[24] Zhu H, Zhang H, Zhou N, Ding J, Jiang J, Liu T, Liu Z, Wang F, Zhang Q, Zhang Z, Yan S, Li L, Benabdallah N, Jin H, Liu Z, Cai L, Thorek DLJ, Yang X and Yang Z. Molecular PET/CT profiling of ACE2 expression in vivo: implications for infection and outcome from SARS-CoV-2. Adv Sci (Weinh) 2021; 8: e2100965.

[25] Joshi S, Balasubramanian N, Vasam G and Jarajapu YP. Angiotensin converting enzyme versus angiotensin converting enzyme-2 selectivity of MLN-4760 and DX600 in human and murine bone marrow-derived cells. Eur J Pharmacol 2016; 774: 25-33.

[26] Beyer D, Vaccarin C, Deupi X, Mapanao AK, Cohrs S, Sozzi-Guo F, Grundler PV, van der Meulen NP, Wang J, Tanriver M, Bode JW, Schibli R and Müller C. A tool for nuclear imaging of the SARS-CoV-2 entry receptor: molecular model and preclinical development of ACE2-selective radiopeptides. EJNMMI Res 2023; 13: 32.

[27] Li X, Li J, Zhou P, Li D, Wang M, Tong Q, Chen J, Zuo C, Zhang L and Li R. The functional views on response of host

rabbit post coronavirus vaccination via ACE2 PET. Am J Nucl Med Mol Imaging 2023; 13: 43-50.
[28] Li X, Yin W, Li A, Li D, Gao X, Wang R, Cui B, Qiu S, Li R, Jia L, Zuo C, Zhang L and Li M. ACE2 PET to reveal the dynamic patterns of ACE2 recovery in an infection model with pseudocorona virus. J Med Virol 2023; 95: e28470.
[29] Zhou L, Zhang R, Yao W, Wang J, Qian A, Qiao M, Zhang Y and Yuan Y. Decreased expression of angiotensin-converting enzyme 2 in pancreatic ductal adenocarcinoma is associated with tumor progression. Tohoku J Exp Med 2009; 217: 123-131.
[30] Tempero MA, Malafa MP, Al-Hawary M, Behrman SW, Benson AB, Cardin DB, Chiorean EG, Chung V, Czito B, Del Chiaro M, Dillhoff M, Donahue TR, Dotan E, Ferrone CR, Fountzilas C, Hardacre J, Hawkins WG, Klute K, Ko AH, Kunstman JW, LoConte N, Lowy AM, Moravek C, Nakakura EK, Narang AK, Obando J, Polanco PM, Reddy S, Reyngold M, Scaife C, Shen J, Vollmer C, Wolff RA, Wolpin BM, Lynn B and George GV. Pancreatic adenocarcinoma, version 2.2021, NCCN clinical practice guidelines in oncology. J Natl Compr Canc Netw 2021; 19: 439-457.
[31] Matsumoto I, Shirakawa S, Shinzeki M, Asari S, Goto T, Ajiki T, Fukumoto T, Kitajima K and Ku Y. 18-Fluorodeoxyglucose positron emission tomography does not aid in diagnosis of pancreatic ductal adenocarcinoma. Clin Gastroenterol Hepatol 2013; 11: 712-718.
[32] Okano K, Kakinoki K, Akamoto S, Hagiike M, Usuki H, Yamamoto Y, Nishiyama Y and Suzuki Y. 18F-fluorodeoxyglucose positron emission tomography in the diagnosis of small pancreatic cancer. World J Gastroenterol 2011; 17: 231-235.
[33] Lee JW, Kang CM, Choi HJ, Lee WJ, Song SY, Lee JH and Lee JD. Prognostic value of metabolic tumor volume and total lesion glycolysis on preoperative ^{18}F-FDG PET/CT in patients with pancreatic cancer. J Nucl Med 2014; 55: 898-904.
[34] Arundhathi A, Chuang WH, Chen JK, Wang SE, Shyr YM, Chen JY, Liao WN, Chen HW, Teng YM, Pai CC and Wang CH. Prorenin receptor acts as a potential molecular target for pancreatic ductal adenocarcinoma diagnosis. Oncotarget 2016; 7: 55437-55448.
[35] George AJ, Thomas WG and Hannan RD. The renin-angiotensin system and cancer: old dog, new tricks. Nat Rev Cancer 2010; 10: 745-759.
[36] Ishiguro S, Yoshimura K, Tsunedomi R, Oka M, Takao S, Inui M, Kawabata A, Wall T, Magafa V, Cordopatis P, Tzakos AG and Tamura M. Involvement of angiotensin II type 2 receptor (AT2R) signaling in human pancreatic ductal adenocarcinoma (PDAC): a novel AT2R agonist effectively attenuates growth of PDAC grafts in mice. Cancer Biol Ther 2015; 16: 307-316.
[37] Lam KY and Leung PS. Regulation and expression of a renin-angiotensin system in human pancreas and pancreatic endocrine tumours. Eur J Endocrinol 2002; 146: 567-572.
[38] Donoghue M, Hsieh F, Baronas E, Godbout K, Gosselin M, Stagliano N, Donovan M, Woolf B, Robison K, Jeyaseelan R, Breitbart RE and Acton S. A novel angiotensin-converting enzyme-related carboxypeptidase (ACE2) converts angiotensin I to angiotensin 1-9. Circ Res 2000; 87: E1-9.
[39] Santos RA, Simoes e Silva AC, Maric C, Silva DM, Machado RP, de Buhr I, Heringer-Walther S, Pinheiro SV, Lopes MT, Bader M, Mendes EP, Lemos VS, Campagnole-Santos MJ, Schultheiss HP, Speth R and Walther T. Angiotensin-(1-7) is an endogenous ligand for the G protein-coupled receptor Mas. Proc Natl Acad Sci U S A 2003; 100: 8258-8263.
[40] Santos RA and Campagnole-Santos MJ. Central and peripheral actions of angiotensin-(1-7). Braz J Med Biol Res 1994; 27: 1033-1047.
[41] Krishnan B, Torti FM, Gallagher PE and Tallant EA. Angiotensin-(1-7) reduces proliferation and angiogenesis of human prostate cancer xenografts with a decrease in angiogenic factors and an increase in sFlt-1. Prostate 2013; 73: 60-70.
[42] Menon J, Soto-Pantoja DR, Callahan MF, Cline JM, Ferrario CM, Tallant EA and Gallagher PE. Angiotensin-(1-7) inhibits growth of human lung adenocarcinoma xenografts in nude mice through a reduction in cyclooxygenase-2. Cancer Res 2007; 67: 2809-2815.
[43] Ni L, Feng Y, Wan H, Ma Q, Fan L, Qian Y, Li Q, Xiang Y and Gao B. Angiotensin-(1-7) inhibits the migration and invasion of A549 human lung adenocarcinoma cells through inactivation of the PI3K/Akt and MAPK signaling pathways. Oncol Rep 2012; 27: 783-790.
[44] Qian YR, Guo Y, Wan HY, Fan L, Feng Y, Ni L, Xiang Y and Li QY. Angiotensin-converting enzyme 2 attenuates the metastasis of non-small cell lung cancer through inhibition of epithelial-mesenchymal transition. Oncol Rep 2013; 29: 2408-2414.
[45] Li D, Ding J, Liu TL, Wang F, Meng XX, Liu S, Yang Z and Zhu H. SARS-CoV-2 receptor binding domain radio-probe: a non-invasive approach for angiotensin-converting enzyme 2 mapping in mice. Acta Pharmacol Sin 2022; 43: 1749-1757.
[46] Parker MFL, Blecha J, Rosenberg O, Ohliger M, Flavell RR and Wilson DM. Cyclic (68)Ga-labeled peptides for specific detection of human angiotensin-converting enzyme 2. J Nucl Med 2021; 62: 1631-1637.
[47] Zhang Q, Liu T, Ding J, Zhou N, Yu Z, Ren Y, Qin X, Du P, Yang Z and Zhu H. Evaluation of (68)Ga- and (177)Lu-labeled HZ20 angiotensin-converting enzyme 2-targeting peptides for tumor-specific imaging. Mol Pharm 2022; 19: 4149-4156.
[48] Ma W, Fu F, Zhu J, Huang R, Zhu Y, Liu Z, Wang J, Conti PS, Shi X and Chen K. (64)Cu-labeled multifunctional dendrimers for targeted tumor PET imaging. Nanoscale 2018; 10: 6113-6124.
[49] Lewis MR, Wang M, Axworthy DB, Theodore LJ, Mallet RW, Fritzberg AR, Welch MJ and Anderson CJ. In vivo evaluation of pretargeted 64Cu for tumor imaging and therapy. J Nucl Med 2003; 44: 1284-1292.
[50] Mushtaq S, Bibi A, Park JE and Jeon J. Recent progress in technetium-99m-labeled nanoparticles for molecular imaging and cancer therapy. Nanomaterials (Basel) 2021; 11: 3022.
[51] Tavares AA and Tavares JM. (99m)Tc Auger electrons for targeted tumour therapy: a review. Int J Radiat Biol 2010; 86: 261-270.
[52] Ku A, Facca VJ, Cai Z and Reilly RM. Auger electrons for cancer therapy - a review. EJNMMI Radiopharm Chem 2019; 4: 27.
[53] Zhang Q, Lu S, Li T, Yu L, Zhang Y, Zeng H, Qian X, Bi J and Lin Y. ACE2 inhibits breast cancer angiogenesis via suppressing the VEGFa/VEGFR2/ERK pathway. J Exp Clin Cancer Res 2019; 38: 173.

[54] Song J, Han J, Liu F, Chen X, Qian S, Wang Y, Jia Z, Duan X, Zhang X and Zhu J. Systematic analysis of coronavirus disease 2019 (COVID-19) receptor ACE2 in malignant tumors: pan-cancer analysis. Front Mol Biosci 2020; 7: 569414.

[55] Ko YJ, Kim WJ, Kim K and Kwon IC. Advances in the strategies for designing receptor-targeted molecular imaging probes for cancer research. J Control Release 2019; 305: 1-17.

[56] Zhou L, Zhang R, Zhang L, Yao W, Li J and Yuan Y. Angiotensin-converting enzyme 2 acts as a potential molecular target for pancreatic cancer therapy. Cancer Lett 2011; 307: 18-25.